Electron Backscatter Diffraction of Nb_3Sn Coated Niobium: Revealing Structure as a Function of Depth

J. Tuggle[1a)], U. Pudasaini[2], J. Angle[1], G. Eremeev[3], C.E. Reece[3], F.A. Stevie[4]
M.J. Kelley[1,2,3]

[1]Virginia Polytechnic Institute and State University, Blacksburg, VA, USA

[2]The College of William and Mary, Williamsburg, VA, USA

[3]Thomas Jefferson National Accelerator Facility, Newport News, VA, USA

[4]Analytical Instrumentation Facility, North Carolina State University, Raleigh, NC, USA

[a)]Electronic Mail: JaysMail@vt.edu

Over the last two decades, advances in Electron Backscatter Diffraction (EBSD) have moved the technique from a research tool to an essential characterization technique in many fields of material research. EBSD is the best suited technique for determining structure as a function of depth. This characterization is critically important, but has been previously absent from Nb_3Sn efforts. While EBSD is the technique of choice, obtaining quality data can be difficult. Sample preparation in particular is non-trivial. Here we summarize the general principles of EBSD, discuss specific sample preparation techniques for Nb_3Sn coated SRF cavity material, and give examples of how EBSD is being used to understand fundamental growth mechanisms for Nb_3Sn coatings.

1 Introduction

1.1 Motivation for Work with SRF Materials

High energy particle accelerators are an invaluable tool in the effort to expand the frontier of science and in order to expand further, more powerful accelerators must be constructed.

Currently, the base technology for these high energy research accelerators utilizes solid niobium superconducting radio frequency (SRF) resonating cavities. The construction and operational cost of the cryogenics plants required can make new more powerful accelerators prohibitively expensive. In order to push accelerators further the cost of cryogenics must be reduced. From a materials perspective, one of the leading next generation technologies is the development of a well understood and robust Nb_3Sn coating process. Nb_3Sn coated cavities have several advantages over solid niobium cavities, including a higher critical temperature and a theoretically higher accelerating gradient. This would allow for warmer (4.2 K vs 2 K) accelerator operation and physically smaller accelerators, both of which positively affect build and operational costs.

It has been more than 40 years since accelerator science researchers started exploring Nb_3Sn as an alternative to solid niobium cavities. [1] However, there still is not full understanding of the coating and growth process, how this affects material structure, or translates to cavity performance. Secondary ion mass spectrometry (SIMS) has proved the technique of choice for analysis of composition as a function of depth for SRF cavity materials. [2] However, in addition to elemental composition, it is necessary to reveal the materials structure over meaningful depths. In the case of current coatings this can range from near surface to 5 µm or more in depth. For this size scale, EBSD is suited better than any other instrumentation available. Here, we will provide an overview of the technique, sample preparation methods specific for SRF cavity materials and example data from Nb_3Sn coating experiments and investigations.

1.2 Electron Backscatter Diffraction

EBSD is a fairly young technique, with the first fully automated commercial systems becoming available in the mid 1990's. [3] The technique quickly progressed and showed exponential

growth in literature as instruments became available in the early 2000's. [4] Today it is often the technique of choice for microstructural analysis of crystalline materials. Grain size and shape, misorientation between and within grains, phase content, defects, and texture results such as inverse pole figures can be obtained from a single analysis. In addition, if installed as an integrated Energy Dispersive Spectroscopy (EDS) and EBSD system as the instrument employed here, data can be combined with elemental information. Commonly a Focused Ion Beam (FIB) is also added to the same platform.

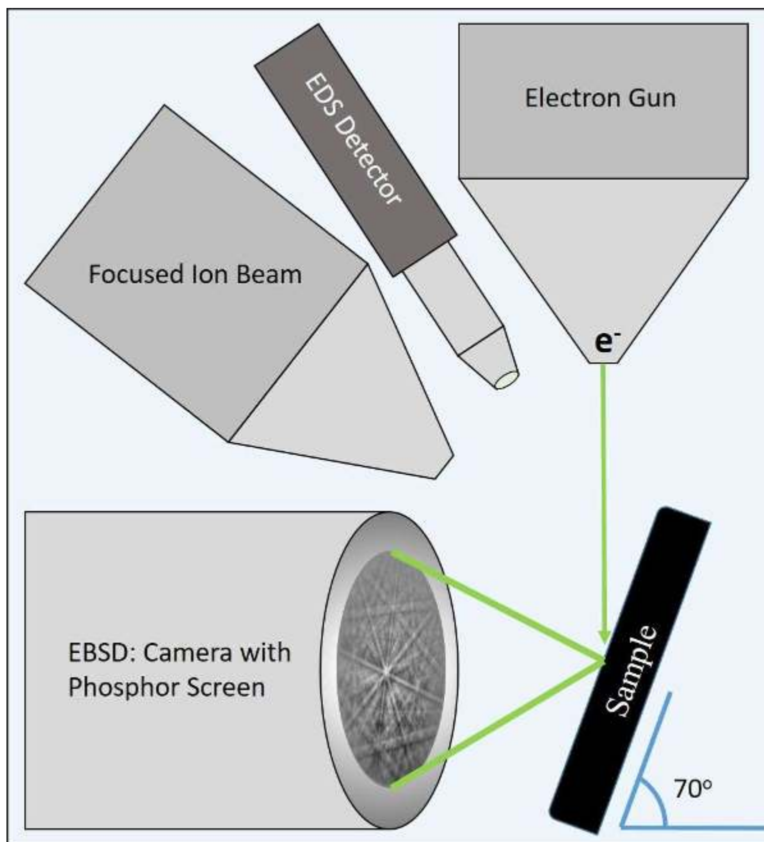

Figure 1.1 Configuration of dual beam microscope equipped with EDS, EBSD, and FIB.

EBSD instrumentation is an addition to a scanning electron microscope (SEM). The main hardware component of the EBSD system is a phosphor screen and charge-coupled device (CCD) configured as illustrated in Figure 1.1. The sample is mounted tilted towards the phosphor

screen at an angle that creates an e^- incidence angle of ~20°. This geometry is suitable to observe diffraction patterns and maximizes the number of backscattered electrons able to escape the sample surface.

Bragg's law describes the process, shown schematically in Figure 1.2. Electrons scatter in all directions from within the interaction volume. Figure 1.2 shows the path of one scattered electron is $2d \sin \theta$ longer than the other, making them out of phase. These path differences lead to constructive and destructive interference. [5] A fraction of the electrons satisfy Bragg's equation by scattering at an appropriate angle (θ). This is the condition for constructive interference, creating high intensity cones of electrons, Kossel cones, to form. Where the Kossel cones intersect the phosphor screen, Kikuchi lines and a lattice specific diffraction pattern (Kikuchi pattern) are formed. Figure 1.3 shows a Kikuchi pattern collected from niobium bulk material.

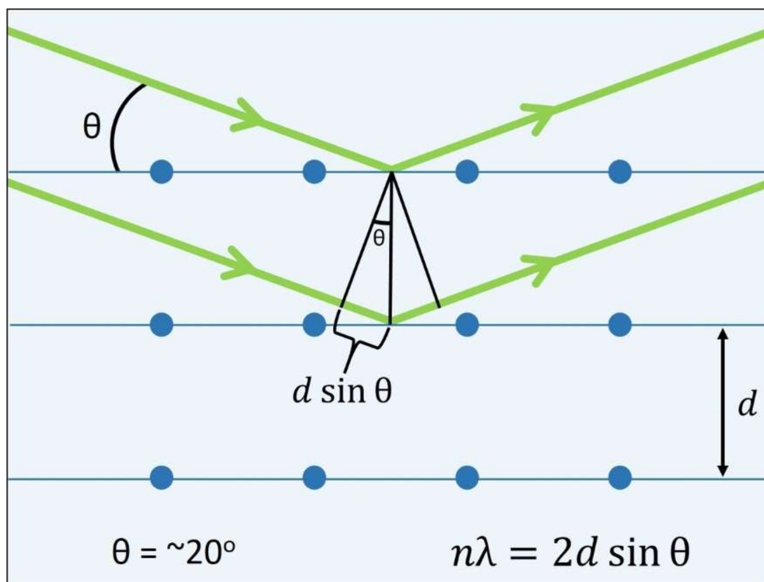

Figure 1.2 Schematic showing diffraction from crystal planes and indicating geometry involved in Bragg's equation.

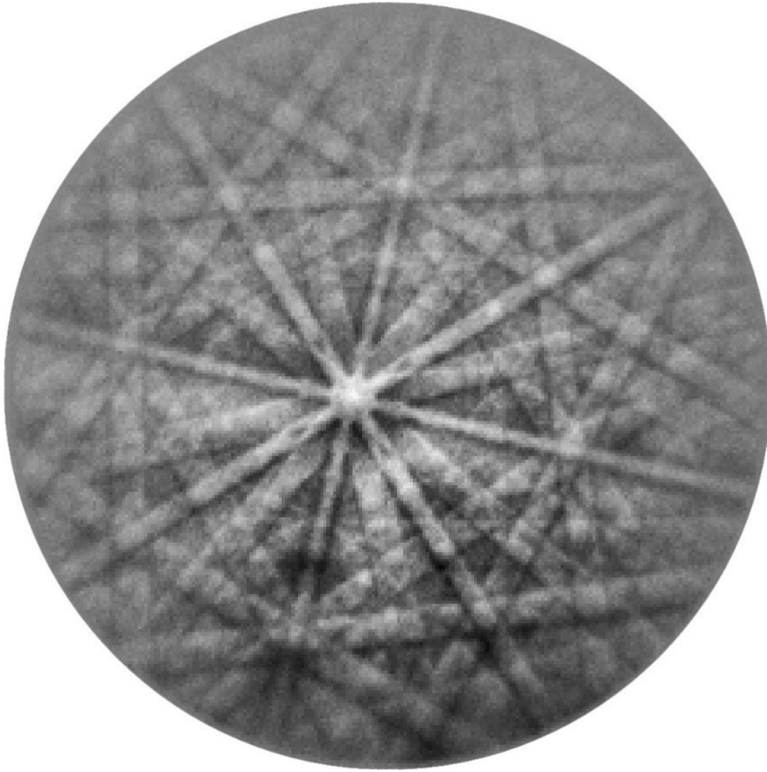

Figure 1.3 Kikuchi pattern collected from bulk niobium after vibratory polishing.

The diffraction pattern formed is a 2D trace of the materials lattice structure, with the width of the Kikuchi bands corresponding to the lattice spacing. The patterns can therefore be used to determine the material's phase and orientation, or "indexed". The rate of indexing patterns has impressively increased to above 1,000 frames per second for commonly available instrumentation or higher for state-of-the-art instrumentation. [6, 7, 8] This has moved map collection from hours/map to maps/hour, making for a logistically favorable characterization technique.

2 Experimental

2.1 Materials

Unless otherwise stated, samples were 10 mm square coupons cut by electrical discharge machining from trimmings of the 3 mm thick niobium sheet used to make SRF cavities ("RRR grade"). Typical grain size for polycrystalline material is in the 50 μm to 100 μm range in the un-annealed state. All were subjected to buffered chemical polishing (BCP) using a solution of 49% HF, 70% HNO_3 and 85% H_3PO_4 in the ratio of 1:1:1 by volume with minimum removal of 50 μm. These samples further received metallographic polishing, also known as nanopolishing (NP) [9], which typically removes > 100 μm and produces surface roughness on the order of a few nanometers. [10] Nb_3Sn coatings were prepared using the vapor deposition process. Several examples include coatings grown on niobium which was anodized prior to the coating. For in-depth discussion of the Nb_3Sn vapor deposition setup, process, and anodization refer to reference [11].

2.2 Electron Backscatter Diffraction

EBSD was performed via FEI NanoLab 600 dual beam, which is equipped with an integrated EDS/EBSD collection system, including an EDAX TSL EBSD camera and Octane Elite EDS with 25 mm^2 detector. Data processing was performed using EDAX OIM Analysis and NIH ImageJ software.

2.2.1 Analysis Conditions

There is no universal "best" EBSD condition and parameters for analysis are dependent upon material type and the goals of the analysis. [12] Typical EBSD conditions range in beam voltages from 10-30 kV and beam currents of 1-50 nA at ~20° incidence angle. [13, 5] Optimal conditions

for pattern indexing of Nb_3Sn with a 2 kV surface polish (see section 2.2.7) were found to be 30 kV and 5.5 nA with an incidence angle of ~14°. This lower incidence angle increases interaction volume while decreasing depth, which reduces lateral resolution, but helps to increase the signal to noise ratio. Depending on the quality of the surface it may be necessary to raise the electron beam current in order to increase the signal to noise ratio and help with indexing quality. Beam currents up to 21 nA (the maximum current for the particular instrument) were used successfully with acceptable lateral resolution.

2.2.2 Data Density

When collecting orientation maps that will be used for quantitative analysis, such as grain size, it is important to consider beam raster step size. While smaller step size (higher resolution) images in theory produce more accurate results, this is not always the case or logistically possible when analyzing real world samples. As step size gets smaller the number of data points and subsequently the time required for analysis goes up exponentially. Longer collection times can cause error from both physical drift and drift caused by charging. Longer collection times also lead to more contamination in the form of carbon buildup on the sample surface, causing weaker signal and indexing issues. [14] Choosing the largest acceptable step size which will clearly describe the sample is recommended. For relatively simple quantification, such as average grain size, 8-10 steps (~100 points) per grain are recommended [15, 12, 4]. More intricate characterization, such as interface, defect, or precipitate characterization will necessitate lower step sizes. When performing investigatory work on samples of unknown feature size, smaller step sizes are necessary to insure features of importance are not left unresolved. Typical step sizes for analysis here range from approximately 0.02 µm to 1.0 µm, depending on the size of the map and detail needed.

Figure 2.1 Magnified grain boundary from bulk niobium in Figure 2.2B, each pixel represents a 30 nm step.

2.2.3 Lateral Resolution

Lateral resolution can vary greatly, depending on microscope type (field emission sourced microscopes result in smaller values than a tungsten source), primary beam energy (higher energies result in higher values), material (higher density materials result in lower values), and collection parameters (step size). Ultimate lateral resolution is commonly reported to range from 5-200 nm. [13, 5, 16, 4] Effective resolution is dependent upon the software system's ability to deconvolute overlapping patterns of neighboring volumes [16]. The effective resolution can be calculated using the fraction of indexed to non-indexed points (see Ref. [15] for details). Here, because EDS was used in conjunction to aid indexing and only two phases were present, indexing is close to 100%, resulting in calculated resolutions of ~0 nm. In this case the effective resolution can be estimated from the smoothness of the grain boundaries. [17] Figure 2.1 shows a

magnified grain boundary from Figure 2.2B, where the mapping step size, i.e. pixel size, is 30 nm. Based on this, the effective resolution for Figure 2.2B is estimated at 60 nm.

2.2.4 Data Cleaning

Kikuchi patterns collected are not necessarily of high enough quality/contrast to be indexed well. This results in either non-indexed or incorrectly indexed points. Non-indexed points will appear as black pixels in a map. A large number of non-indexed points can be seen in both Figure 2.2A and Figure 3.4B. Incorrectly indexed points rarely form in cubic metals (incorrect indexing is more common in low-symmetry materials) and appear as isolated, highly misoriented pixels. [15] Several incorrectly indexed points can be seen along the grain boundary in Figure 2.1. If a sufficient number of data points are not indexed or mis-indexed cleaning steps can be performed to remove erroneous points. There are many algorithms (nearest neighbor, average orientation, minimum/maximum grain size, misorientation, etc) included with most analysis software in order to facilitate easy cleaning of data. Care must be taken in using data cleaning and it should be used lightly as to not misrepresent the data collected. Samples such as Nb_3Sn coatings are good candidates for a "light" cleaning as sample preparation can be quite difficult and time consuming. For example, a common problem with Nb_3Sn coating preparation is contamination with niobium which has been redeposited from the bulk material. This can be very difficult or logistically not feasible to completely eliminate. In this study, cleaning was applied using either grain size limits, a single phase per grain filter, grain dilation, or combination of the three. The goal is to clean without distorting the results by only replacing a small percentage of the total data collected. Cleaning steps were limited to replacing ~10% or less of the displayed data in order to preserve the integrity of the analysis.

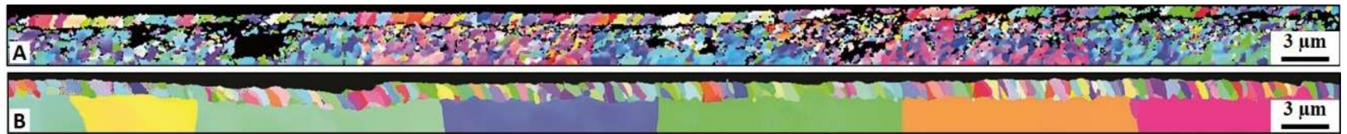

Figure 2.2 Two examples of EBSD cross sections (approximately 85 µm in length). Figure 2.2A shows a nanopolished sample, while Figure 2.2B shows a cross section prepared by diffuse ion beam.

2.2.5 Sample Preparation

Similar to lateral resolution, information depth varies widely with accelerating voltage, material density, etc. Information depth in silicon has been shown to be less than 40 nm, dropping to ~10 nm for the heavier element Ni at 20 kV. [17] With comparable accelerating voltages information depths of 10 nm or less can be expected for niobium and Nb_3Sn. When working with such shallow depths of information, the selection and implementation of sample preparation method are of high consequence. Sample preparation consumes the vast majority of the time required for method development and work required in the performance of EBSD. Because of the shallow information depth of the technique the surface must be free from contamination and residual deformation. Any significant amount of amorphous surface layer, such as deformation from mechanical preparation, surface oxides from exposure to atmosphere, or surface contamination as a result of beam interaction can degrade or prevent observation of diffraction patterns. It has been reported as little as 3 nm of amorphous material will cause pattern degradation. [14]

Metal specimens prepared with normal metallographic techniques require further polishing to reduce the deformation layer. [3] Typically, vibratory polish with a colloidal silica suspension in the size range of 0.02 µm is sufficient for a final polish. Nb_3Sn coated niobium cross sections prove particularly difficult due to the soft nature of niobium, hardness difference between niobium and Nb_3Sn, and edge retention needed at both the Nb_3Sn/Nb interface and Nb_3Sn

surface. It was found prohibitively difficult and impractical to achieve EBSD results by mechanical only polishing. Cross section samples were sent for professional metallographic polishing using a proprietary technique referred to as "nanopolishing" (NP). [9] NP samples have been used for coating experiments and SIMS analysis previous with great success and found well suited for characterization experiments. [18, 19, 20] EBSD results from a NP cross section are shown in Figure 2.2A. While the NP polished sample provided the first published EBSD results for Nb_3Sn coated SRF cavity niobium, there are issues which needed to be resolved. [21] The first issue is that the bulk niobium is known to be relatively large grain (~10-100 μm) material. However, Figure 2.2A shows each niobium grain made up of many (<1 μm) micro-grains. In addition, large patches of data failed to index and are missing in both the niobium and Nb_3Sn phases of the map. Maybe most importantly there is no indexed data found at the Nb_3Sn/Nb interface. These problems are attributed to damage and topography caused by the NP technique.

Sample preparation issues were resolved by combining an initial mechanical polish with a final polish via ion beam. During ion polishing, ions (Ar and Ga for this work) are accelerated towards the sample with sufficient energy to remove material from the surface. Care must be taken when choosing polishing parameters. High impact energies and angles can lead to thick damage layers, while high currents can lead to sample heating. Properly implemented ion beam techniques were found to perform well, giving high quality surfaces excellent for EBSD analysis. Both diffuse ion beam and focused ion beam (FIB) techniques were utilized with great success.

Figure 2.3 Leica TIC 3x sample chamber with triple argon ion beams. Sample location is at beam convergence point.

2.2.6 Diffuse Ion Beam Polishing

Diffuse ion beam polishing was accomplished via a Leica EM TIC 3x milling system. The TIC 3x makes us of three loosely focused argon ion guns in order to polish a relatively large area. The TIC 3x sample chamber with three argon ion beams can be seen in Figure 2.3.

Since the ion beams are diffuse in nature, care must be taken mounting and masking the sample in a way to protect the surface and uniformly sputter material away over the area of interest. Normally masking the surface is a straightforward process involving the placement of the sample surface up to a tungsten carbide mask placed perpendicular to the beam path. Anything above the mask will be removed, leaving an ion polished cross-section. This standard mounting can be seen in Figure 2.4A. In the case of Nb_3Sn, the natural roughness of the surface was found to prevent the mask from making a proper fit (Figure 2.4B), resulting in turbulent argon flow, failing to protect the surface, and leaving a large amount of topography through the Nb_3Sn layer. Several mounting geometries and embedding techniques were tested and the following technique was

found to produce the highest quality results. Two small pieces of the sample were glued surface to surface using M-Bond 610 adhesive. A small clamping vise was used in order to insure square bonding with a minimal amount of glue between samples, thus creating a sandwich with the area of interest in the middle. The sample was then mounted with the surface junction parallel to the beam direction. The sample face closest to the beam was mechanically polished before mounting in order to ensure a tight square fit to the tungsten carbide mask. (Figure 2.4C)

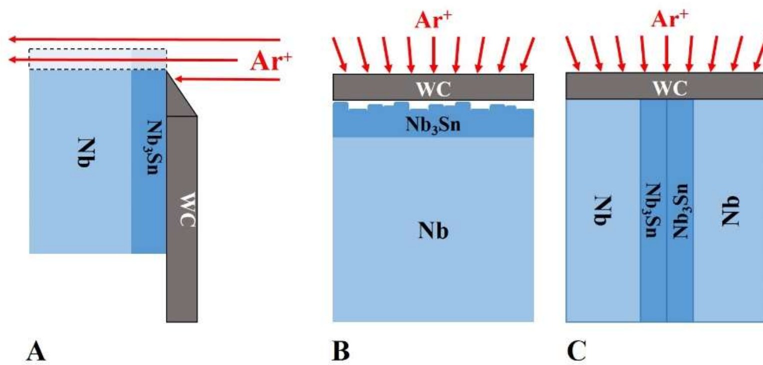

Figure 2.4 Sample mounting for Leica TIC 3x. A.) Cross-section view showing tungsten carbide (WC) mask with standard mounting. B.) Top down view of standard mounting, showing gaps due to rough Nb_3Sn surface. C.) Top down view of sandwich method for mounting.

With ion beam techniques the main determinants of damage depth are accelerating voltage and incidence angle. Best results were found with incidence angles $<10^{\circ}$ and by working stepwise from 10 kV down to ≤ 3 kV. Stepping down the accelerating voltage has the same effect as moving from lower to higher grit sandpaper, successively removing less material and causing less damage with each step. Eventually only a few nm's of damage remain; less than ~3 nm under the above conditions. [22] Using these conditions and the sandwich mounting technique, two (left and right side) samples are created, with EBSD quality areas of several hundred microns in length. Figure 2.2B shows an example of an ion beam polished cross section. The ion beam polished sample shows none of the issues the NP sample did. Large single orientation

grains can be seen in the bulk niobium, while the Nb_3Sn layer and interface region are well indexed.

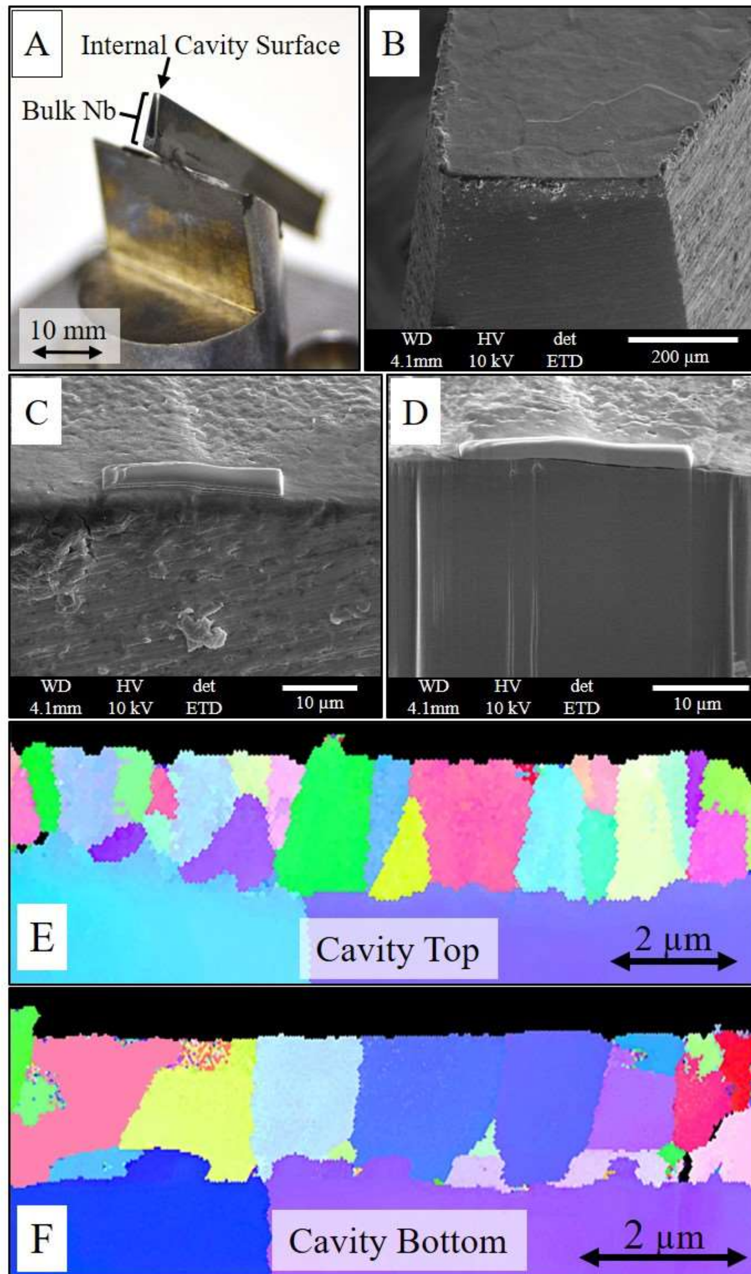

Figure 2.5 (A) Cavity cut-out specimen mounted to SEM stub ready for FIB cross-sectioning and polish (B-D). Example orientation maps from FIB preparation of cavity cut-out specimens (E-F).

2.2.7 Focused Ion Beam Polishing

While diffuse ion polishing via the TIC 3x creates EBSD quality surfaces, sample size and shape are limited and special care has to be taken in sample mounting for even regularly shaped coupons. Sample mounting becomes quite difficult with anything outside of the simplest geometries. For samples with unique geometries or where preparation of specific areas, such as defects, is required, Focused Ion Beam (FIB) becomes the preferred preparation method.

FIB was accomplished with a FEI NanoLab 600 dual beam instrument. The NanoLab makes use of a FIB with Ga source capable of 1-30 kV, with a maximum of 21 nA of current. The general layout can be seen in Figure 1.1. It is quite convenient to have the EBSD system mounted to the dual beam instrument, allowing for final polish and cleaning steps in situ as needed.

While FIB preparation of cross sections yields smaller cross sections and is more complicated in nature than preparation by the TIC 3x, the quality of analysis surface is unsurpassed. Cavity cutouts (segments cut from a wall of an SRF Cavity) are a geometrically complicated example, with compound curved surfaces that can be convex or concave. In addition, cavity cutouts are often small in size. Figure 2.5A shows an example of a small cavity cutout with less than 1 mm of cavity surface available for analysis. The specimen is mounted and electrically grounded appropriately to a 45° SEM specimen mount. The 45° mounting simplifies moving between ion milling and EBSD analysis positions in the FEI system.

For FIB preparation, a cross section should be initially mechanically polished. Starting with a well-polished cross section makes FIB polishing much more efficient and practical, as FIB removes relatively small amounts of material at low rates. When possible, sample faces were polished at a slight negative angle (~3°), leaving less bulk niobium to be removed by FIB. In order to preserve the surface of the Nb_3Sn and create an intact cross section, a protective layer of

platinum is deposited on the sample surface over the cross section's area of interest. Figure 2.5B and Figure 2.5C show SEM images of the cavity specimen, before and after a Pt layer is placed on an area of interest, in this case a niobium grain boundary. Once the Nb_3Sn surface is protected, a similar approach is taken as with TIC polishing, stepping down through accelerating voltages and beam currents, removing smaller and smaller amounts of material, while subsequently causing less damage, until left with a smooth EBSD quality cross section. (Figure 2.5D) Initial material removal steps are performed at the highest removal rate of 30 kV / 21 nA. With a low incidence angle (~1°) and 30 kV accelerating voltage, a damage layer approximately 10 nm in depth is formed. [22] The sample is then rotated and final polishing is performed perpendicular to the cross-sectioned surface. First at 5 kV, followed by 2 kV, at ~90° incidence leaving a damage layer of 3-5 nm. Optimal patterns have only been collected after a 2 kV final polish

3 Results and Discussion

Provided here are qualitative and quantitative examples and brief discussion of how the EBSD technique helps gain a fundamental understanding of the Nb_3Sn coating process. The examples are meant to be illustrative of how EBSD may be applied to real world sample sets. For in-depth discussion of coating mechanism, structure and composition please see U. Pudasaini et al.

3.1 Coating Dependence on Cavity Geometry

The homogenous coating of SRF cavities presents a challenge due to the inherently complicated shape. In order to optimize the coating process data is needed not just from witness samples, but from processed cavities. Figure 2.5E and Figure 2.5F show example orientation maps from FIB prepared cavity cutouts obtained from different locations in a coated cavity. Analyses such as

these can be used to directly determine geometry specific coating issues for large complex SRF cavity shapes. [23] In this case, while the average grain area was not found to be statistically different between "Top" and "Bottom", 1.4(±0.4) µm and 1.6(±0.6) µm respectively, a more bimodal distribution in grain size was seen in the "Top" sample.

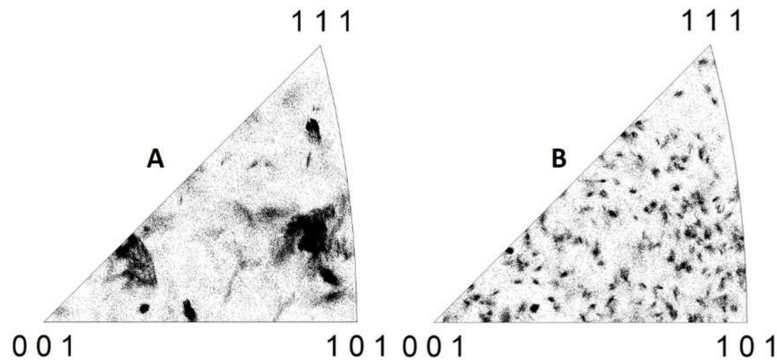

Figure 3.1 IPF of niobium bulk material (A) and the Nb_3Sn coating (B) derived from data in Figure 2.2B.

3.2 Orientation Dependence of Nb_3Sn

One of the open-ended questions at the time of this work was whether Nb_3Sn coatings showed substrate orientation-based preferences. Large cross sections like that shown in Figure 2.2B provide a direct answer through inverse pole figures. An inverse pole figure is a simplified way of exposing preferred crystal orientation or texture based on the stereographic projection. Figure 3.1 shows two inverse pole figures (IPF) from Figure 2.2B, Figure 3.1A of the niobium bulk material and Figure 3.1B of the Nb_3Sn coating. There are approximately six distinct orientations shown in the IPF for the niobium bulk material, consistent with what is seen in Figure 2.2B. Figure 3.1B shows many orientations and no preferred crystal orientation for the Nb_3Sn coating over the same region. IPF data has been collected over many cross sections of both polycrystalline and single crystalline niobium, which had been coated with Nb_3Sn. In no case was a correlation seen between bulk material and coating crystal orientation.

Orientation data can also be used to calculate the misorientation or rotation angle between grains. Figure 3.2A shows an example map of grain boundary misorientation for an Nb_3Sn coated niobium coupon. The color of the lines located along grain boundaries represents the rotation angle between grains. Due to the symmetry in a cubic lattice no two grains can differ by more than ~62.8°. The legend found in Figure 3.2B lists binned rotation angles and their corresponding line color up to 63°. Rotation angles were measured across the Nb/Nb_3Sn interface for ~250 grains from six specimens coated using various times and temperatures. Results are shown via histogram in Figure 3.2C. Nb_3Sn coatings appear to show no specific crystalline orientation via IPF based on bulk niobium crystalline orientation. However, misorientation data shows a preferential rotation angle of ~50° for Nb_3Sn grains formed at the interface.

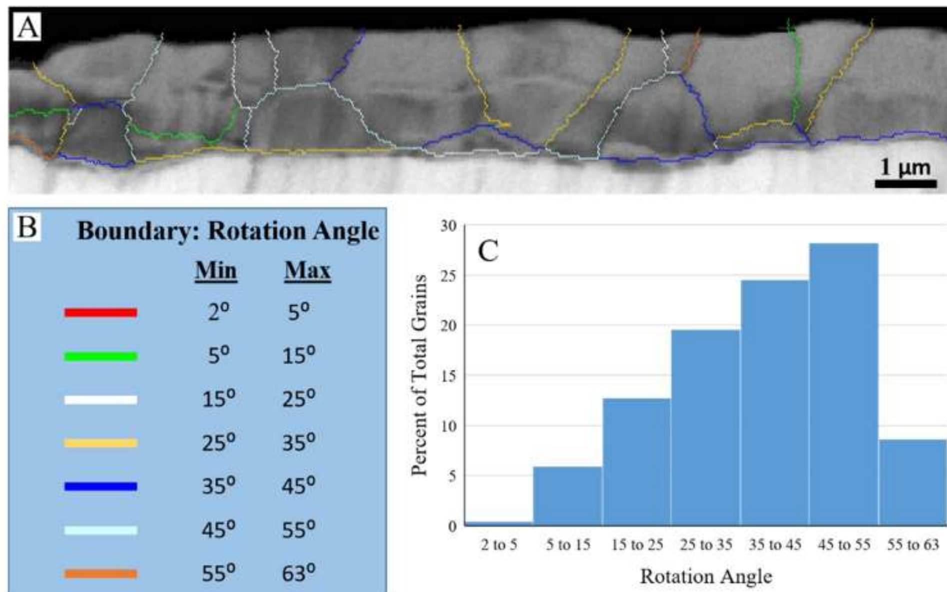

Figure 3.2 (A) Map showing Nb_3Sn coating on niobium with grain boundary misorientation information overlaid. (B) Legend for grain boundary rotation angles. (C) Data collected from ~250 grains located at the Nb/Nb_3Sn interface from multiple samples.

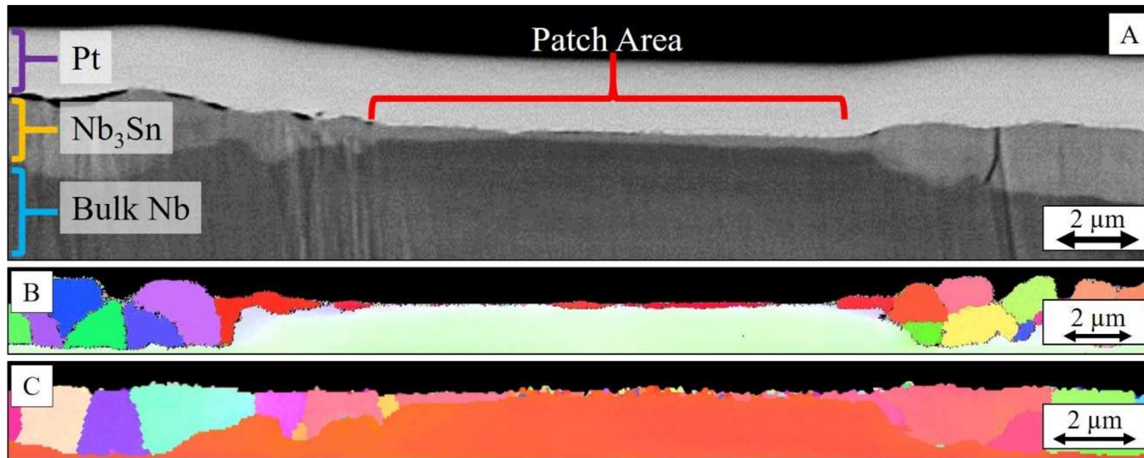

Figure 3.3 (A) SEM image of FIB cross sectioned patch defect. (B-C) Orientation maps of patch defects prepared by FIB.

3.3 Patch Defects

Patches are defects which form during the Nb_3Sn coating process to varying degree across many bulk material, cavity, and coating conditions. [24, 25] EDS surface analysis was reported by others which shows varying Nb/Sn ratio within the patch region with changing accelerating voltage. [26] This variation is indicative of a surface layer with thickness less than the escape depth of characteristic X-rays detected in EDS. The expected escape depth for Nb/Sn at the low end of the reported accelerating voltages is still several hundred nanometers, making it difficult to judge the actual patch thickness.

Here, cross sections from several patch defects from a single coupon were prepared by FIB and imaged by SEM, allowing for direct quantification of the thickness. Patch thickness was found to be 194(±59) nm as compared to overall Nb_3Sn thickness of 1.6(±0.1) µm for the coupon. The reduced thickness within the patch region is of concern due to its relative closeness to the RF penetration depth (~170 nm). An SEM image of a FIB prepared patch cross section can be found in Figure 3.3A.

Example EBSD results from FIB prepared patch cross sections can be found in Figure 3.3B and Figure 3.3C. The patch cross sections clearly show a coating that forms at the niobium surface and progresses downward consuming niobium as tin is made available at the Nb_3Sn/Nb interface. A combination of relatively high beam current, low incidence angle, and possibly damage from polishing leads to the thinnest parts of the patch being unresolved in the EBSD maps shown. However, in all patches observed by SEM the Nb_3Sn layer appeared to be thin, but continuous across the entire patch area.

Surface EBSD analysis of patch afflicted Nb_3Sn was also performed, but is made difficult by the prominent topography of the surface. Figure 3.4 shows an SEM image with corresponding EBSD map. The combination of surface topography and low incidence angle (~20°) of the electron beam required for analysis forms many “shadowed” (black areas in Figure 3.4B) regions where no signal is produced. This produces a noisy surface map; however, the large patch areas are relatively smooth and index well. In agreement with the previously shown cross section EBSD, this map shows the patches are large single grains of Nb_3Sn. Both, cross section and surface analysis indicate that lack of grain boundaries is the limiting factor in coating growth rate for patch areas.

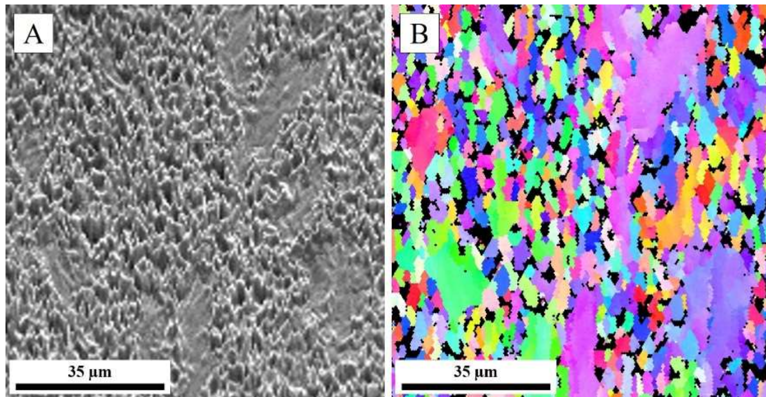

Figure 3.4 SEM image (A) and corresponding orientation map (B) of Nb_3Sn surface area containing patches. Patches index as single crystal Nb_3Sn.

3.4 Surface Anodization Effect on Coating

Recent coating experiments with anodized substrates have indicated a positive effect for the coating uniformity and reduction of patch defects. [27, 28] Other studies involving anodization and the nucleation process have shown mixed results. [11, 29] Here we use EBSD and analysis by NIH ImageJ software to help gain insight into the structural differences between Nb_3Sn grown on anodized niobium surfaces versus that grown on NP niobium surfaces.

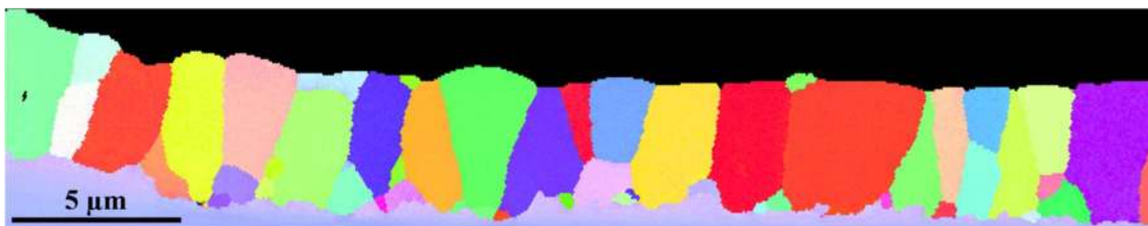

Figure 3.5 EBSD orientation map collected from a sample that was anodized prior to Nb_3Sn coating. (1100 ºC / 12 hr)

Four coated samples were analyzed, two which had been anodized prior to coating and two which had not. Multiple maps were collected from each sample representing 100 – 200 µm of coating from each sample, which equates to ~100 grains of Nb_3Sn per sample. Figure 3.5 shows

an example map collected from a sample anodized prior to Nb_3Sn coating. Comparing samples by average grain size proves difficult due to the large spread in size leading to large standard deviations. Coatings grown for 12 hr at 1100 ºC were found to have an average grain size of 3.31 μm^2 (±3.7) for pre-anodized and 4.45 μm^2 (±4.8) for non-anodized. Viewing grain size as a histogram shows a clearer picture of differences (Figure 3.6), with the two samples showing a slightly different grain size distribution.

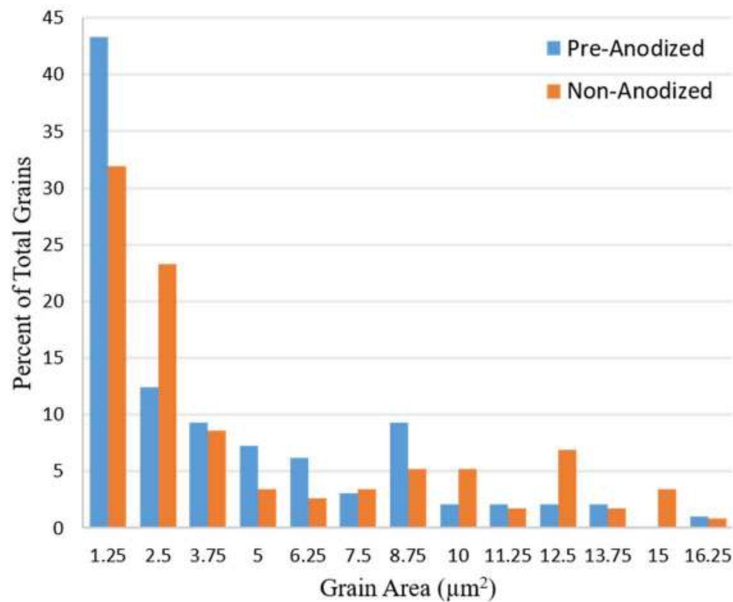

Figure 3.6 Histogram comparing grain size of Nb_3Sn coated samples with and without pre-anodization.

The aspect ratio of each grain was calculated by dividing the major axis by the minor axis of each grain giving a quantified value which represents the elongation of a grain. A perfectly square grain would have an aspect ratio of 1 and as the ratio increases so does the elongation of the grain. Again, a histogram is used to visualize the difference in aspect ratio between pre-anodized and non-anodized samples. (Figure 3.7) The distribution in grain aspect ratios appear very similar, with a preferred aspect ratio of ~1.5. The pre-anodized sample does show a smaller

percentage of grains at the upper end (2.8 – 4.0) and a slightly higher center of distribution at 1.6 versus 1.4 for the non-anodized sample.

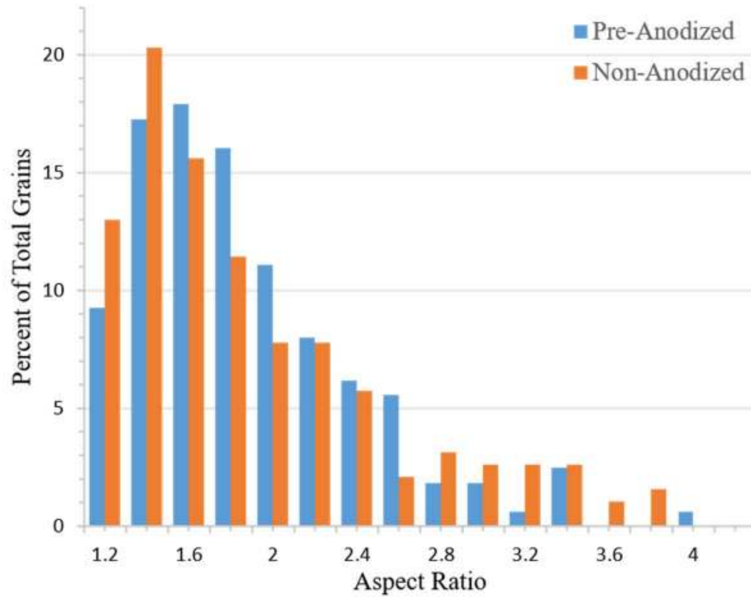

Figure 3.7 Histogram comparing the range of aspect ratio in Nb3Sn coatings with and without pre-anodization.

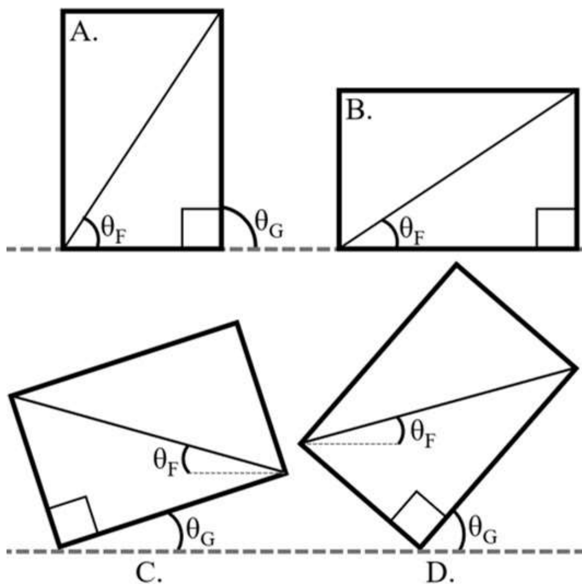

Figure 3.8 Graphic showing relationship of Feret angle to physical geometry of Nb_3Sn grain. Where θ_F is the Feret angle and θ_G is the orientation angle of the grain with respect to the x-axis.

Feret diameter is the longest distance between any two points along a particle's boundary, also described as the largest caliper measurement of the particle. The Feret angle is the angle between the Feret diameter and a line parallel to the x-axis of the image, which in our case is approximately parallel with the Nb/Nb_3Sn interface. It is possible to get some statistical idea of the physical orientation of the grain within the coating using the Feret angle. If we assume a roughly rectangular shaped grain structure the Feret diameter is measured from corner to corner. A perfectly square grain with an aspect ratio of 1 would have a Feret angle of 45° when oriented square to the interface. For Nb_3Sn's preferred aspect ratio of ~1.5 a Feret angle of ~56° would equate to a vertically oriented grain (Figure 3.8A) while an angle of ~34° would equate to a horizontally oriented grain (Figure 3.8B).

Angle distribution, shown in Figure 3.9, appears bimodal. With an aspect ratio of ~1.5 the peak seen at ~60° corresponds to vertically oriented grains. The second peak, seen at ~15°, corresponds with grains which are physically oriented at either a 19° or 49° tilt to the horizontal axis (Figure 3.8C and D). Qualitatively, when viewing maps (Figure 3.5), large grains seem to be vertically oriented while smaller grains contribute to the large peak representing grains with 19° or 49° tilt. When plotted with respect to grain size (Figure 3.10) the bimodal nature of the Feret angle can be seen in smaller grain sizes with larger grains showing Feret angles distributed almost entirely around ~60°. There are several outliers in the non-anodized data set attributable to "muffin-top" grains, where the maximum diameter of the grain is parallel to the niobium substrate, but is still a vertical grain. While these outliers are explained by the presence of large "muffin-top" grains vs large flat grains it is still of note that these do not appear in the pre-anodized samples.

In general, for uniform coating growth and reduction of patch defects, having smaller vertically oriented grains would be beneficial. The data here indicates pre-anodized samples have both. The pre-anodized samples show a larger number of the smallest grains of which a higher percentage appear to be oriented in a vertical direction. This illustrates a possible mechanism for the reduction of patch defects seen in pre-anodized samples.

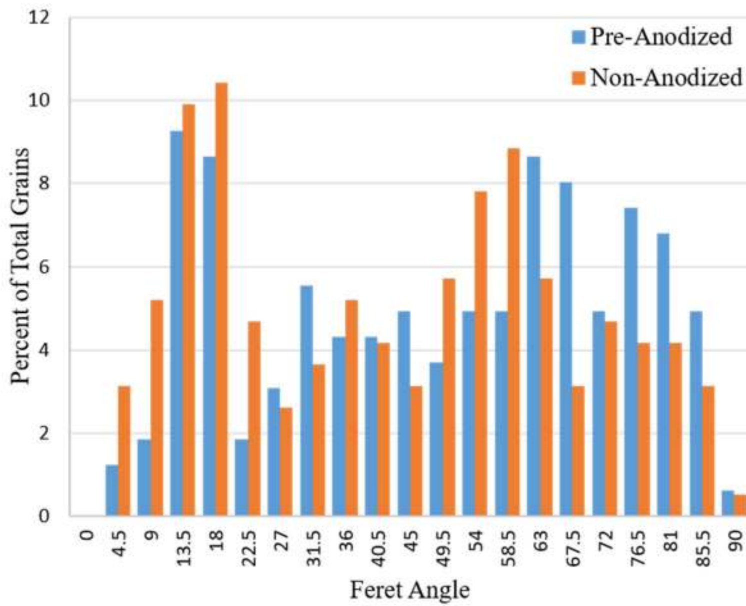

Figure 3.9 Histogram showing the distribution of the Feret angle for coatings grown with and without pre-anodization.

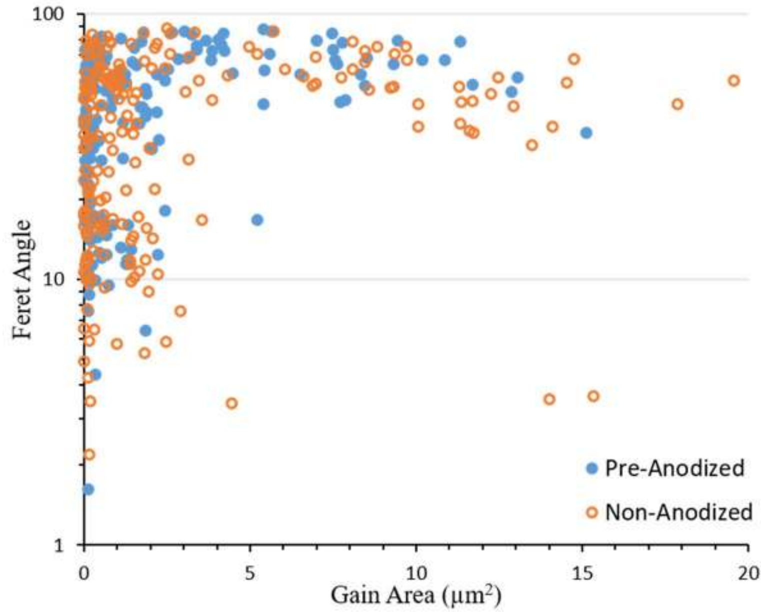

Figure 3.10 Plot showing Feret angle as a function of grain size for coatings grown with and without pre-anodization.

3.5 The Initial Overcoat Experiment

In order to gain insight into the formation and growth of Nb_3Sn films, previously coated coupons were subjected to additional coating and characterized. These coupons were referred to as "overcoat" samples. The overcoat samples were prepared by FIB and characterized by EBSD in cross section. Figure 3.11A shows an example orientation map from as-coated niobium while Figure 3.11B shows a sample which has been coated a second time. The overcoat sample shows the formation of new grains at the Nb_3Sn/Nb interface. This indicates a formation mechanism which includes additional tin diffusion to the interface which initiates additional grain growth, as opposed to the formation of a new surface layer. In addition, grain formation appears to occur more times than not at the intersection of an original Nb_3Sn grain boundary and the niobium interface, indicating grain boundary diffusion as the primary mode for tin movement to the interface. Further evidence of this can be seen in the "cupping" at the base of many Nb_3Sn grains

(Figure 3.11A), showing grain growth faster around the edges of the grain. With grain boundary diffusion as the primary mode of transport of tin to the growth interface, it follows that growth rate is inversely proportional to grain size. This is also supported and clearly seen in the patch defect work (Section 3.3).

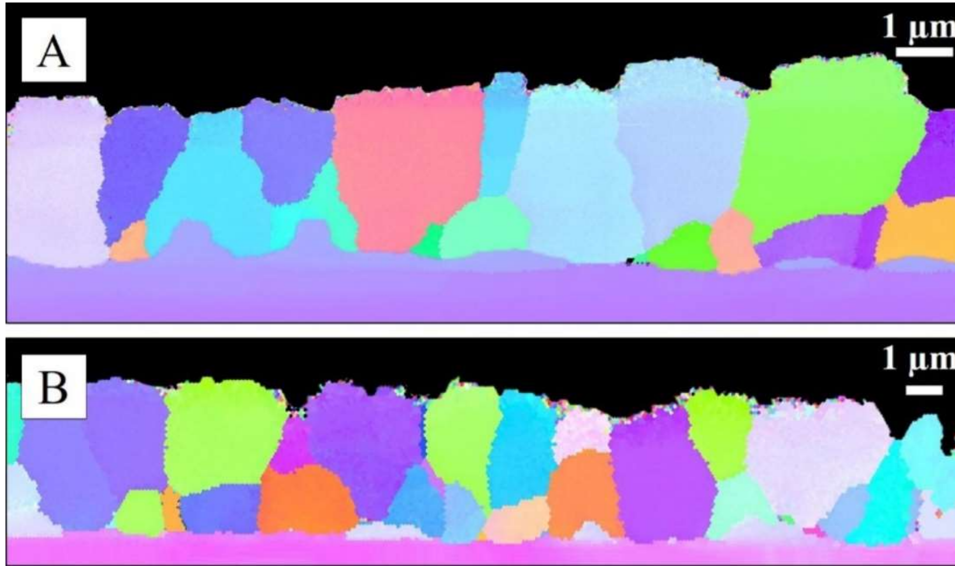

Figure 3.11 Orientation mapping of niobium coated with Nb_3Sn. Map (A) was coated in a single step while map (B) was coated then re-coated. Samples were prepared by FIB.

3.6 Continuation of the Overcoat Experiment

Results from section 3.5 initially seemed clear; overcoating causes more small grains to form at the interface. With time the larger volumes of EBSD data collected qualitatively appear to show small grains at the interface universally present and seemingly independent of coating condition. This suggests a mechanism of coating formation which requires small interfacial grains to be formed and then absorbed by larger grains which make up the bulk of the coating. Laid out below is a quantitative approach to explore this further. Data collected from six coated samples was analyzed. Nb_3Sn coating was performed in steps and total coating time varied with each sample. Table 3.1 shows the six coatings.

Table 3.1 Coating steps for six overcoat samples tested. "1" represents one hour of coating, "1+1" represents one hour of coating plus an additional hour, etc.

Sample	1	2	3	4	5	6
Coating Steps in Hours	1	1+1	1+1+1	1+1+1+3	1+1+1+3+12	1+1+1+3+12+60

Cross sections of each sample were prepared by FIB as described in section 2.2.7. Orientation maps from sample 2, 4, and 6 are shown in Figure 3.12A, B, and C respectively. Each map is limited to 15 µm in length in order to exhibit the large differences in relative grain size between coatings. In each of the three orientation maps, grains of ~1 µm are present. As the coating times increase the size of the grains forming the bulk of the coating also increases. Using NIH ImageJ software, size distribution for each sample was determined. The grain size distribution for sample one is shown in Figure 3.13A. The total coating time for the sample equals one hour and small grains account for 100% of the coating with a maximum grain size measured of 6.4 μm^2. After an additional hour of coating (two hours total) a bimodal distribution in grain size can start to be seen. (Figure 3.13B). Sample 2 had a maximum measured grain size of 10.5 μm^2. This bimodal distribution widens as the total coating time increases eventually ending in the extreme case of Sample 6. (Figure 3.13C). The largest measured grain area for Sample 6 was 183.0 μm^2. Large grains, >15 μm^2, make up a total of 98% of the coating area. Interestingly the number of grains is split approximately evenly between small (48%) and large (52%). Data collected from the six samples seems to confirm the growth mechanism for Nb_3Sn requires small intermediate grains to form at the boundary layer, which then absorb and become part of the bulk coating as growth progresses. Again, for in-depth discussion of coating, mechanism, structure and composition please see U. Pudasaini et al.

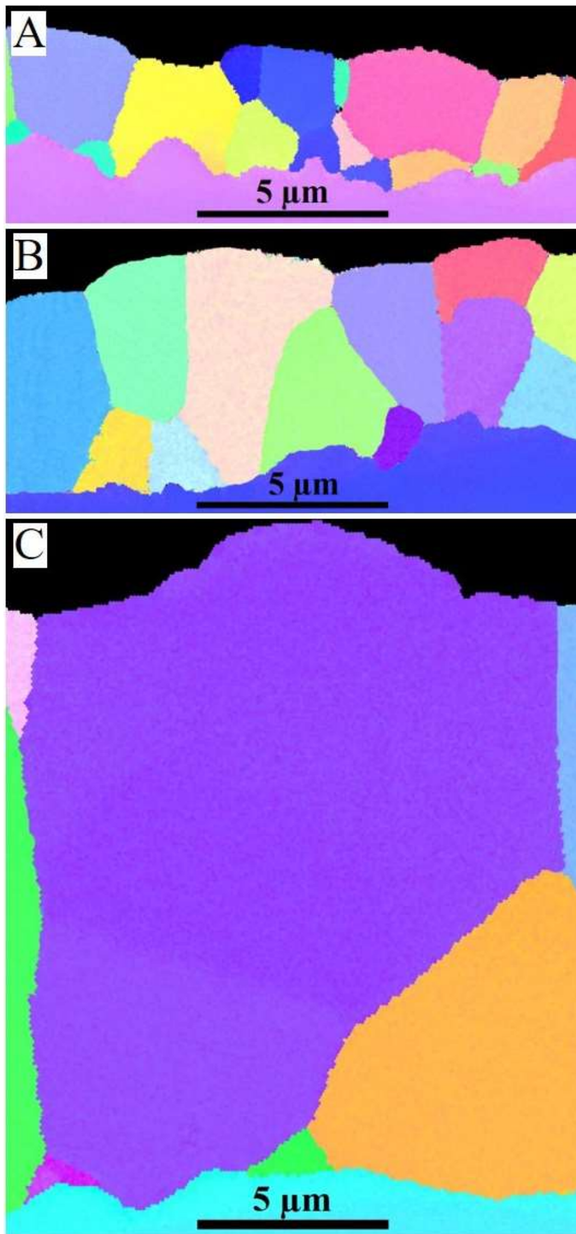

Figure 3.12 Orientation maps A, B, and C, collected from samples 2, 4, and 6 as found in Table 3.1. Each map shows a 15 µm length of Nb_3Sn coating.

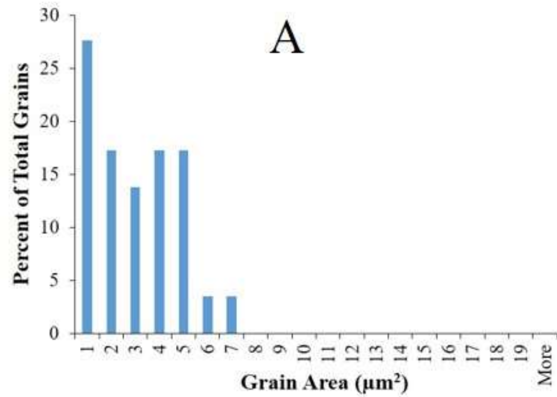

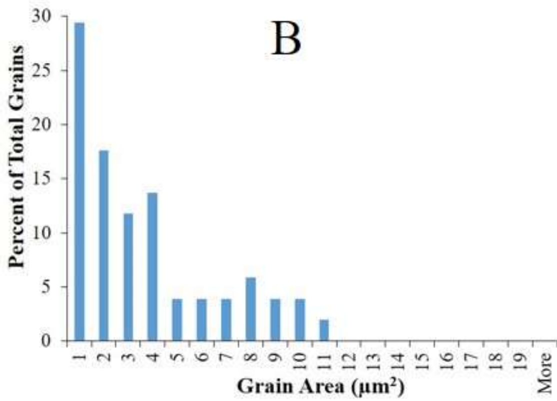

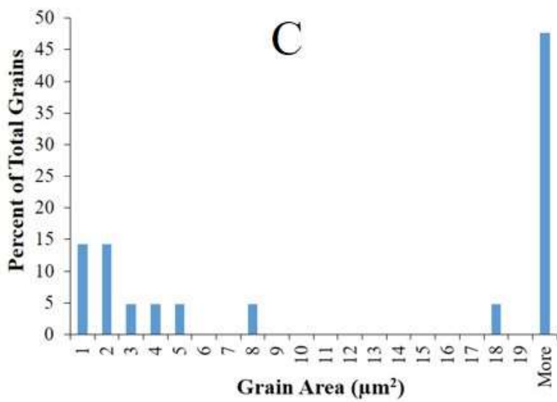

Figure 3.13 Histograms A, B, and C are grain size distributions for samples 1, 2, and 6 as found in Table 3.1.

4 Conclusion

This work has shown EBSD is the method of choice to visualize and quantify structure as a function of depth for Nb_3Sn coated SRF cavity material. Some of the results have been

disseminated. [21, 30] Ion beam sample preparation methods were found to perform best for EBSD quality surface finishes. Diffuse ion beam polishing, accomplished here via the Leica TIC 3x, was successful to create large analysis areas with 100's of microns of usable area. Thus far, EBSD analysis over many hundreds of microns of coating on both polycrystalline and single crystal samples has shown no preferred crystal orientation based on the bulk niobium substrate. Complimentary to diffuse ion polishing, FIB preparation works well in the case of small or geometrically complicated samples. To this point, example analyses were shown from cavity cutout samples which exhibit EBSD's ability to determine structure for complicated geometries, making it possible to directly compare differing areas of coated cavities or target specific defect types.

Work with patch defects indicates Nb_3Sn forms at the Nb_3Sn/Nb interface, progressing "downward" and consuming bulk niobium as tin is made available at the interface through grain boundary diffusion. This implies patches arise from the formation of large single crystal grains early in the coating process. Due to a lack of grain boundaries, the interface is starved of Sn inhibiting further growth of Nb_3Sn in the patch area.

Following the idea of a growth process which is dependent on grain boundaries for growth, aspect ratio, physical grain orientation, and grain size will play a large part in coating rate and uniformity. EBSD and image analysis software were used to quantify these parameters in pre-anodized and non-anodized Nb_3Sn coatings. While further investigation is outside the scope of this work, the differences indicated, namely smaller and more vertically oriented grains, may help elucidate pre-anodizing's ability to reduce patch defects.

5 Acknowledgment

Co-Authored by Jefferson Science Associates, LLC under U.S. DOE Contract No. DE-AC05-06OR23177. We are grateful for support from the Office of High Energy Physics, U.S. Department of Energy under grant DE-SC0014475 to the College of William & Mary.

We would also like to thank the Institute for Critical Technology and Applied Science (ICTAS), and Nanoscale Characterization and Fabrication Laboratory (NCFL) at Virginia Tech

Bibliography

[1] B. Hillenbrand, H. Martens, H.Pfister, K. Schnitzke and Y. Uzel, "Superconducting Nb3Sn Cavities with High Microwave Qualities," *Transactions on Magnetics,* Vols. MAG-13, no. No. 1, pp. 491-495, 1977.

[2] J. Tuggle, U. Pudasaini, A. Palczewski, C. Reece, F. Stevie and M. Kelley, "Secondary Ion Mass Spctrometry for SRF Cavity Materials," *Journal of Vacuum Science and Technology B,* vol. 36, no. 5, 2018.

[3] D. Stojakovic, "Electron Backscatter Diffraction in Materials Characterization," *Processing and Application of Ceramics,* vol. 6, no. 1, pp. 1-13, 2012.

[4] V. Randle, "Electron Backscatter Diffraction: Strategies for Reliable Data Acquisition and Processing," *Materials Characterization,* vol. 60, pp. 913-922, 2009.

[5] T. Maitland and S. Sitzman, Chapter exert from "Scanning Microscopy for Nanotechnology Techniques and Applications", Springer, 2007.

[6] R. Borrajo-Pelaez and P. Hedstrom, "Recent Developements of Crystallographic Analysis Methods in the Scanning Electron Microscope for Applications in Metallurgy," *Critical Reviews in Solid State and Materials Sciences,* pp. 1-20, 2017.

[7] T. Britton, J. Jiang, Y. Guo, A. Vilalta-Clemente, D. Wallis, L. Hansen, A. Winkelmann and A. Wilkinson, "Tutorial: Crystal Orientations and EBSD - Or which way is up?," *Materials Characterization,* vol. 117, pp. 113-126, 2016.

[8] A. Wilkinson, G. Moldovan, T. Britton, A. Bewick, R. Clough and A. Kirkland, "Direct Detection of Electron Backscatter Diffraction Patterns," *Physical Review Letters,* vol. 111, no. 6, 2013.

[9] *Wah Chang proprietary polishing process.*

[10] U. Pudasaini, M. Kelley, G. Eremeev and C. Reece, "Local Composition and Topography of Nb3Sn Diffusion Coatings on Niobium," in *17th International Conference on RF Superconductivity*, Whistler, BC, Canada, 2015.

[11] U. Pudasaini, G. Eremeev, J. T. C.E. Reece and M. Kelley, "Initial Growth of Tin on Niobium for Vapor Diffusion Coating of Nb3Sn," *Superconductor Science and Technology,* vol. Accepted, 2019.

[12] A. Wilkinson and T. Britton, "Strains, Planes, and EBSD in Materials Science," *Materials Today,* vol. 15, no. 9, 2012.

[13] A. Schwartz and B. A. M. Kumar, Electron Backscatter Diffraction in Materials Science, Springer, 2009.

[14] K. Baba-Kishi, "Review Electron Backscatter Kikuchi Diffraction in the Scanning Electron Microscope for Crystallographic Analysis," *Journal Of Materials Science,* vol. 37, pp. 1715-1746, 2002.

[15] F. Humphreys, "Review Grain and Subgrain Characterization by Electron Backscatter Diffraction," *Journal of Materials Science,* vol. 36, pp. 3833-3854, 2001.

[16] S. Zaefferer, "A Critical Review of Orientation Microscopy in SEM and TEM," *Crystal Research and Technology,* vol. 46, no. 6, pp. 607-628, 2011.

[17] D. Dingley, "Progressive Steps in the Developement of Electron Backscatter Diffraction and Orientation Imaging Microscopy," *Journal of Microscopy,* vol. 21, no. 3, pp. 214-224, 2003.

[18] F. Stevie, "SRF Niobium Characterization Using SIMS and FIB-TEM," in *AIP Conference Proceedings*, 2015.

[19] J. Tuggle, A. Palczewski, C. Reece, F. Stevie and M. Kelley, "Investigation of Low-Level Nitrogen in Niobium by Secondary Ion Mass Spectrometry," in *Proceedings of LINAC 2016*, East Lansing, 2016.

[20] J. Tuggle, U. Pudasaini, A. Palczewski, C. Reece, F. Stevie and M. Kelley, "Fundamental SIMS Analyses for Nitrogen Enriched Niobium," in *SRF Conference Proceedings*, Lanzhou, 2017.

[21] J. Tuggle, G. Eremeev, C. Reece, H. Xu and M. Kelley, "Structure and Composition of Nb3Sn Diffusion Coated Films on Nb," in *Proceedings of SRF 2015*, Whistler, 2015.

[22] SRIM, *Stopping Range of Ions In Matter [Software],* www.SRIM.org, ver: SRIM 2013.00.

[23] U. Pudasaini, G. Eremeev, C. Reece, J. Tuggle and M. Kelley, "Examination of Cutouts Inner Surfaces From Nb3Sn Coated Cavity," *Proceedings of LINAC,* 2016.

[24] S. Posen, Writer, *Nb3Sn SRF Coatings at FermiLab.* [Performance]. NAPAC, 2016.

[25] S. Posen, A. Romanenko, Y. Trenikhina, O. Melnychuk and D. Sergatskov, "Cutout Study of a Nb3Sn Cavity," in *Poceedings of SRF2015*, Whistler, BC, 2015.

[26] D. Hall, J. Kaufman, M. Liepe and J. Maniscalco, "Surface Analysis Studies of Nb3Sn Thin Films," in *IPAC 2016 Proceedings*, Busan, Korea, 2016.

[27] U. Pudasini, G. Eremeev, M. Kelley, C. Reece and J. Tuggle, "Surface Studies of Nb3Sn Coated Samples Prepared Under Different Coating Conditions," in *18th International Conference on RF Superconductivity*, Lanzhou, 2017.

[28] D. Hall, M. Liepe, R. Porter, T. Arias, P. Cueva, D. Liarte, D. Muller, J. Sethna and N. Sitaraman, "High Performance Nb3Sn Cavities," in *18th International Conference on RF Superconductivity*, Lanzhou, 2017.

[29] D. Hall, *New Insights into the Limitations on the Efficiency and Achievable Gradients in Nb3Sn SRF Cavities,* PhD Thesis Cornell University, 2017.

[30] J. Tuggle, U. Pudasini, G. Eremeev, A. Palczewski, C. Reece and M. Kelley, "Materials Characterization for SRF Cavities: Gaining Insight Into Nb3Sn," in *IPAC Conference Proceedings*, Copenhagen, 2017.